PROCEEDINGS OF SCIENCE

Searches for Hadronic Resonances at CMS

David Yu[*†]
Brown University
E-mail: david_yu@brown.edu

New particles decaying to jet pairs, predicted by many theories of physics beyond the Standard Model, could be discovered at the Large Hadron Collider as resonances in the dijet invariant mass spectrum. Three searches for dijet resonances by the CMS Collaboration are presented, which employ several novel techniques to probe a wide range of resonance masses. The first search targets resonance masses above 1800 GeV. A new background method using jet pairs with large pseudorapidity separation is described. The latter two searches target resonances below 450 GeV, where trigger bandwidth limitation preclude the methods used at high masses. The resonances are required to be produced with high transverse momentum due to significant initial state radiation (ISR), and hence the resonance decay products are collimated into a single jet. The searches, which require either ISR jets or photons, probe resonance masses from 50 GeV – 450 GeV and 10 GeV – 125 GeV, respectively.

7th Annual Conference on Large Hadron Collider Physics - LHCP2019
20-25 May, 2019
Puebla, Mexico

[*]Speaker.
[†]On behalf of the CMS collaboration

PoS(LHCP2019)184

1. Introduction

New hadronic resonances are predicted by many theories of physics beyond the Standard Model (SM). New particles such as additional gauge bosons [1, 2], excited quarks [3, 4], or Randall-Sundrum gravitons [5] could be discovered at hadron colliders as resonances in the dijet invariant mass spectrum. Searches for such resonances thus have a long tradition at hadron colliders, including the Large Hadron Collider (LHC) [6]. At the LHC, however, the ever-increasing instantaneous luminosity and the corresponding increases in trigger thresholds have pushed the mass range for traditional dijet searches to well above 1 TeV [7, 8]. Several new techniques have been developed to maintain sensitivity to lower mass resonances. During Run 1, the use of trigger-level data, i.e. the jets reconstructed by the high-level trigger algorithms, enabled resonance masses as low as 450 GeV to be probed [9, 10]. Triggers with online b tagging have probed as low as 325 GeV [11]. More recently, searches for resonances produced with large initial state radiation (ISR) have probed as low as 10 GeV.

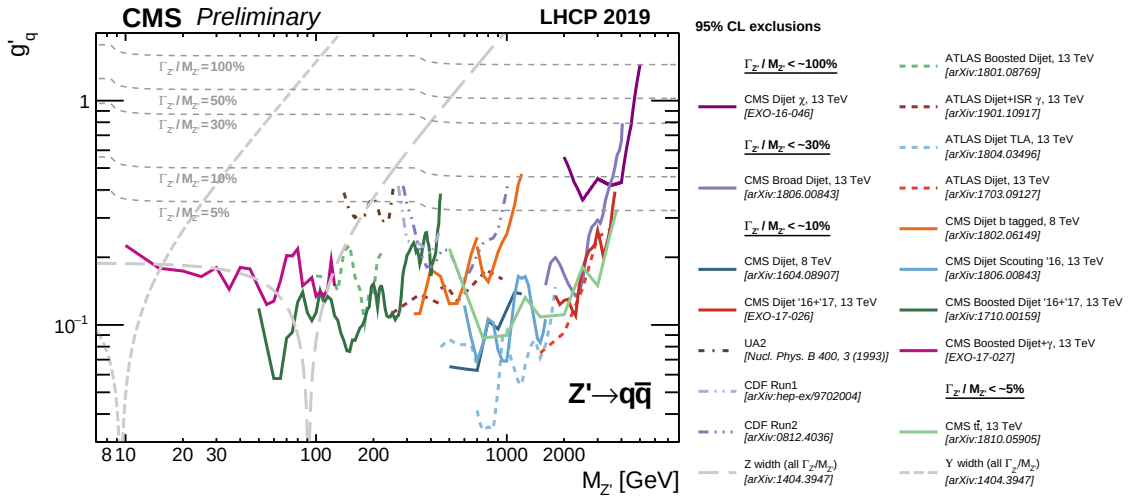

Figure 1: Limits on the universal coupling g'_q between a leptophobic Z′ boson and quarks [2] from various dijet analyses from CMS, ATLAS, CDF, and UA2. The limits are shown in solid lines, with the excluded area above the lines. The hashed areas show the direction of the excluded area from the observed limits. The grey dashed lines show the g'_q values at fixed values of $\Gamma_{Z'}/M_{Z'}$. Most of the analyses, with the exception of Dijet χ and Broad Dijet, assume that the intrinsic width is negligible compared to the experimental resolution, and hence are valid for $\Gamma_{Z'}/M_{Z'} \lesssim 10\%$. The $t\bar{t}$ resonance analysis is valid for $\Gamma_{Z'}/M_{Z'} \lesssim 5\%$, the Broad Dijet analysis is valid for $\Gamma_{Z'}/M_{Z'} \lesssim 30\%$, and the Dijet χ analysis is valid for $\Gamma_{Z'}/M_{Z'} \lesssim 100\%$. Also shown are indirect constraints on g'_q from the Υ and Z boson widths, which are valid for all values of $\Gamma_{Z'}/M_{Z'}$.

These techniques can be compared in the context of a simplified model containing a leptophobic, spin-1 Z' boson, with equal vector couplings to quarks [2]. The Lagrangian for the model is:

$$\mathscr{L} \ni g'_q \sum_{i=1}^{6} Z'_\mu \bar{q}_i \gamma^\mu q_i. \tag{1.1}$$

Figure 1 shows limits on g'_q from UA2, CDF, ATLAS, and CMS, as well as indirect constraints from Υ decays and the hadronic width of the Z boson [12]. The LHC results span three orders of magnitude in resonance mass, from 10 GeV to 8 TeV. Proceeding from high masses to low, the traditional dijet search, using fully reconstructed events, probes masses above ~ 1.5 TeV. With this method, the only cut with a significant impact on the signal acceptance is the requirement on pseudorapidity separation between the two jets, $|\Delta\eta_{jj}| < 1.1$. Assuming that the resonance couples uniformly to all flavors of quarks, searches for $\mathrm{t\bar{t}}$ resonances have similar sensitivity in this range. For masses above 450 GeV, the traditional dijet methods can be applied to trigger-level events, where reduced event size allows for lower trigger thresholds. Between 250 GeV and 450 GeV, the best limits are from searches targeting resonances produced with large ISR, reconstructed as two narrow, resolved jets. If we again assume that the resonance couples uniformly to all flavors of quarks, searches employing online b tagging have similar sensitivity in the range 325 GeV – 450 GeV. Finally, for masses in the range 10 GeV – 250 GeV, searches for resonances with large transverse momentum due to ISR photons and jets have demonstrated unique sensitivity. In this phase space, the resonance decay products are collimated due to the large Lorentz boost, and thus are reconstructed as a single large-radius jet.

This report presents several new strategies developed during Run 2 by the CMS experiment which improve the sensitivity to lower resonance masses and smaller coupling values, pushing the mass coverage as low as 10 GeV. In particular, we describe two searches for dijet resonances produced with high transverse momentum due to significant initial state radiation [13, 14], as well as a new background estimation technique for the high mass search [15].

2. The CMS Detector and Jet Reconstruction

The central feature of the CMS apparatus is a superconducting solenoid of 6 m internal diameter, providing a magnetic field of 3.8 T. Within the solenoid volume are a silicon pixel and strip tracker, a lead tungstate crystal electromagnetic calorimeter (ECAL), and a brass and scintillator hadron calorimeter (HCAL), each composed of a barrel and two endcap sections. Forward calorimeters extend the pseudorapidity coverage provided by the barrel and endcap detectors. Muons are detected in gas-ionization chambers embedded in the steel flux-return yoke outside the solenoid. A more detailed description of the CMS detector, together with a definition of the coordinate system used and the relevant kinematic variables, can be found in Ref. [16].

The particle-flow (PF) algorithm [17] attempts to reconstruct and identify each individual particle in an event, with an optimized combination of information from the various elements of the CMS detector. The energy of photons is obtained from the ECAL measurement. The energy of electrons is determined from a combination of the electron momentum at the primary interaction vertex as determined by the tracker, the energy of the corresponding ECAL cluster, and the energy sum of all bremsstrahlung photons spatially compatible with originating from the electron track. The energy of muons is obtained from the curvature of the corresponding track. The energy of charged hadrons is determined from a combination of their momentum measured in the tracker and the matching ECAL and HCAL energy deposits, corrected for zero-suppression effects and for the response function of the calorimeters to hadronic showers. Finally, the energy of neutral hadrons is obtained from the corresponding corrected ECAL and HCAL energies.

The analyses described here utilize jets formed from PF candidates. Narrow jets are reconstructed with the anti-k_{T} algorithm [18] with a distance parameter of $R = 0.4$ (AK4). Wider jets, which aim to capture the decay products of massive particles with large Lorentz boost, are reconstructed with the anti-k_{T} algorithm with $R = 0.8$ (AK8), or the Cambridge-Aachen algorithm with $R = 1.5$ (CA15) [19]. The algorithms are implemented in the `FastJet` package [20]. The jet momentum is determined as the vectorial sum of all particle momenta in the jet, and is found from simulation to be, on average, within 5 to 10% of the true momentum over the whole p_{T} spectrum and detector acceptance. Jet energy corrections are derived from simulation studies so that the average measured response of jets becomes identical to that of particle level jets. In situ measurements of the momentum balance in dijet, photon+jet, Z+jet, and multijet events are used to determine any residual differences between the jet energy scale in data and in simulation, and appropriate corrections are made [21]. Contributions to the jet momentum from additional proton-proton interactions within the same or nearby bunch crossings are mitigated using the charged hadron subtraction (CHS) or pileup per particle identification (PUPPI) algorithms [22].

3. High mass dijet search

Proceeding from high resonance masses to low, we first present the search for dijet resonances at high mass, using $77.8\,\mathrm{fb}^{-1}$ collected by the CMS detector [15]. The search targets narrow resonances decaying to two jets, with masses greater than 1800 GeV. This threshold is determined by the triggers used to collect events online, which require events to contain one or more jets with large transverse momenta. The analysis uses AK4 CHS jets. The two leading jets in p_{T} are chosen as the resonance decay candidates. To recover potential wide-angle radiation from the final-state partons, additional AK4 jets within a distance of $\Delta R < 1.1$ of the leading two jets are added to the nearest leading jet. We refer to the resulting objects as "wide jets." The two resulting wide jets are each required to have $p_{\mathrm{T}} > 30\,\mathrm{GeV}$ and $|\eta| < 2.5$, and the jet pair must satisfy $|\Delta\eta| < 1.1$. The latter cut selects events with more central jets, and is imposed for two reasons: first, it improves the signal sensitivity, and second, it improves the efficiency of the trigger selection.

The background, dominantly due to QCD multijet events, is estimated in two ways. For $m_{jj} < 2.4\,\mathrm{TeV}$, the background model is a smoothly falling, empirical function, which is fitted to the observed m_{jj} spectrum ("fit method"). The function is given by:

$$\frac{\mathrm{d}\sigma}{dm_{jj}} = \frac{P_0(1-x)^{P_1}}{x^{P_2+P_3\ln(x)}}, \tag{3.1}$$

where $x = m_{jj}/\sqrt{s}$.

For $m_{jj} > 2.4\,\mathrm{TeV}$, the background is estimated from a new technique using events with $|\Delta\eta| > 1.1$ ("ratio method"). Three regions are defined: the signal region with $|\Delta\eta| < 1.1$ (SR), a validation control region with $1.1 < |\Delta\eta| < 1.5$ ($\mathrm{CR}_{\mathrm{middle}}$), and the background control region with $1.5 < |\Delta\eta| < 2.5$ ($\mathrm{CR}_{\mathrm{high}}$). The QCD background prediction in the signal region is taken from $\mathrm{CR}_{\mathrm{high}}$, multiplied by a transfer factor from simulation:

$$N(m_{jj})^{\text{Prediction}}_{\text{SR}} = R_{\text{ext.}} \times N(m_{jj})^{\text{Data}}_{\text{CR}_{\text{high}}} \tag{3.2}$$

$$R_{\text{ext.}} = \text{Corr}(m_{jj}) \times \frac{N(m_{jj})^{\text{Simulation}}_{\text{SR}}}{N(m_{jj})^{\text{Simulation}}_{\text{CR}_{\text{high}}}}. \tag{3.3}$$

The correction factor, parametrized as $\text{Corr}(m_{jj}) = a + b(m_{jj}/\sqrt{s})^4$, accounts for differences in the transfer factor between data and simulation, and is fit to the double ratio $\frac{N(m_{jj})^{\text{Data}}_{\text{CR}_{\text{middle}}}}{N(m_{jj})^{\text{Data}}_{\text{CR}_{\text{high}}}} / \frac{N(m_{jj})^{\text{Simulation}}_{\text{CR}_{\text{middle}}}}{N(m_{jj})^{\text{Simulation}}_{\text{CR}_{\text{high}}}}$.

Figure 2 shows the observed m_{jj} spectrum, along with the background predictions from the two methods and reference shapes for quark-quark, quark-gluon, and gluon-gluon signal models. No significant excess is observed. Upper limits on the product of the cross section (σ), the branching fraction to dijets (B), and the detector acceptance (A) are shown in figure 3. The local significance of the data for quark-quark resonances is shown in figure 4; note that the signficances for the ratio method are generally higher than those from the fit method, reflecting the reduced systematic uncertainty of the method.

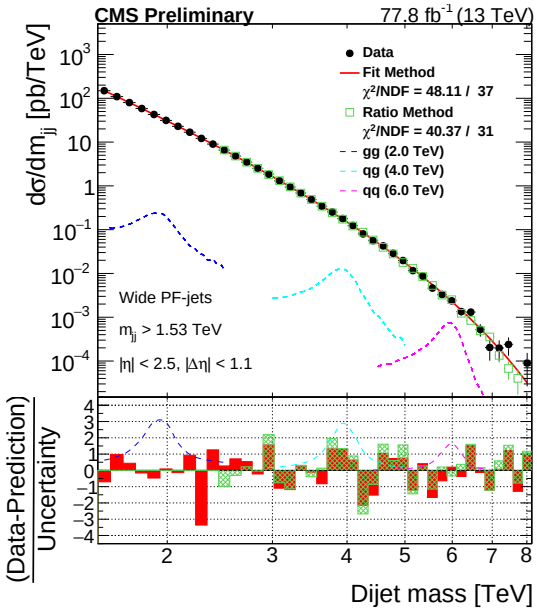

Figure 2: Dijet mass spectra in the signal region (points) compared to a fitted parameterization of the background (solid curve) and the one obtained from the control region (green squares). For the displayed signal a cross section at the 95% CL observed exclusion limit is being used. The lower panel shows the difference between the data and the fitted parametrization (red), and the data and the prediction obtained from the control region (green), divided by the statistical uncertainty of the data, which for the ratio method includes the one in CR_{high} as well. The ratio of the expected signal showed in the upper panel to the statistical uncertainty of the data is also shown for three different resonance masses and signals models.

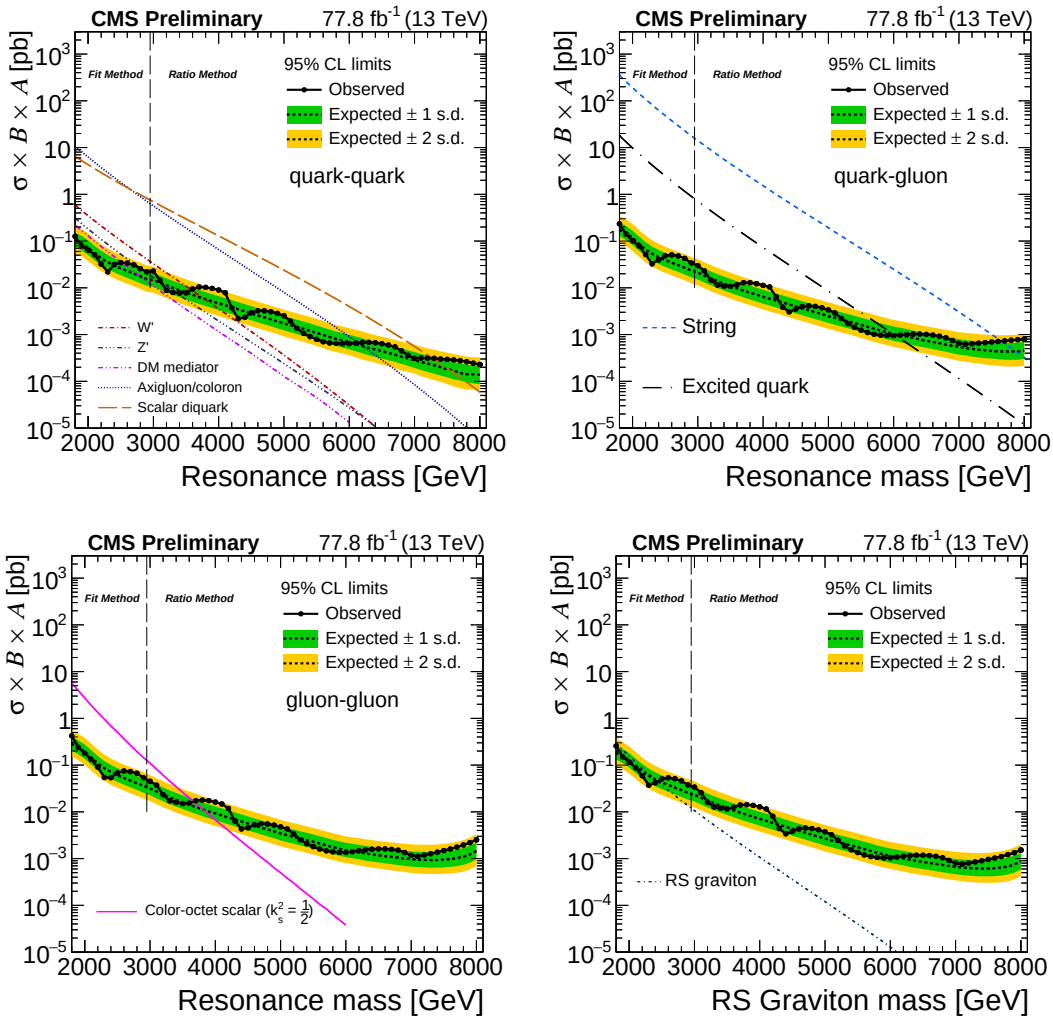

Figure 3: The observed 95% CL upper limits on the product of the cross section, branching fraction, and acceptance for dijet resonances decaying to quark-quark (top left), quark-gluon (top right), gluon-gluon (bottom left), and for RS gravitons (bottom right). The corresponding expected limits (dashed) and their variations at the 1 and 2 standard deviation levels (shaded bands) are also shown. Limits are compared to predicted cross sections for string resonances, excited quarks, axigluons, colorons, scalar diquarks, color-octet scalars, new gauge bosons W' and Z' with SM-like couplings, dark matter mediators for mDM= 1 GeV, and RS gravitons.

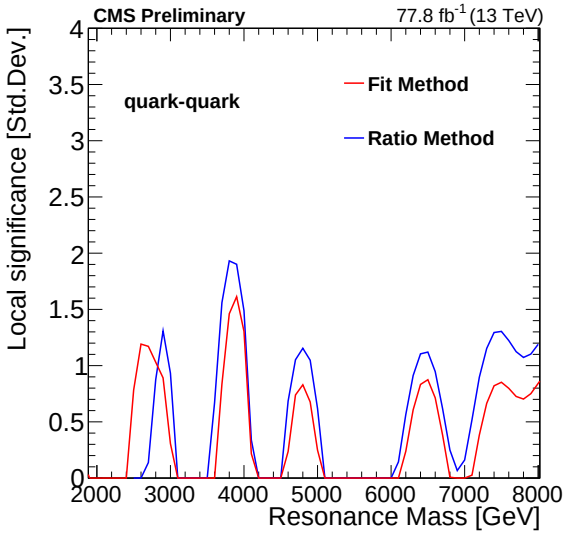

Figure 4: Local significance for a narrow resonance from the fit method (red) and the ratio method search (blue) for qq resonances.

4. Boosted dijet search with ISR jets

The high-mass dijet resonance search probes resonance masses in the range 1800 GeV – 8000 GeV; as mentioned previously, trigger-level analysis techniques allow the range to be extended down to about 450 GeV. To probe even lower masses, a more radical change in approach is needed to circumvent the trigger bandwidth limitations. The strategy which provides the best sensitivity in the range 10 GeV – 450 GeV is to require that the resonance be produced with significant ISR [14, 23, 24, 25]. We now present a search for Z′ resonances produced with high transverse momentum due to ISR jets, using an integrated luminosity of 77.0 fb^{-1} [13]. Due to the significant Lorentz boost, the resonance decay products are collimated into a single, large-radius jet. Using triggers that select events containing a large-radius jet with high mass and high transverse momentum, the search probes dijet resonance masses in the range 50 GeV – 450 GeV.

The search uses large-radius AK8 or CA15 jets built from PF candidates. The PUPPI algorithm is applied to reduce the impact of pileup interactions. AK8 jets, employed in both 2016 and 2017 data, are used for smaller resonance masses, where the decay products are more collimated. CA15 jets are only used in 2017 data, and improve the sensitivity at larger resonance masses. The triggers employ only AK8 jets, requiring that the event contain at least one jet with large trimmed mass [26], $m_{\text{trim}} > 30$ GeV, and untrimmed $p_{\text{T}} > 380$ GeV – 400 GeV. The signal candidate is taken to be the AK8 or CA15 jet with the highest p_{T}. The AK8 jets are required to have $p_{\text{T}} > 500$ GeV (2016) or $p_{\text{T}} > 525$ GeV (2017), due to different trigger thresholds in the two years. CA15 jets are required to have $p_{\text{T}} > 575$ GeV. The jet must also satisfy $|\eta| < 2.5$.

Jet substructure information is used to discriminate the signal from the dominant QCD background. The soft-drop mass algorithm [27], with $\beta = 0$ and $z_{\text{cut}} = 0.1$, removes soft and wide-angle radiation from the jet. The resulting soft-drop mass, m_{SD}, tends to be significantly reduced for QCD jets, while the mass of jets due to Z′ candidates (as well as top quarks and W and Z bosons)

is preserved. The p_T-invariant variable $\rho \equiv \log(m_{SD}^2/p_T^2)$ is required to satisfy $-5.5 < \rho < -2.0$ ($-4.7 < \rho < -1.0$) for AK8 (CA15) jets, to avoid non-perturbative effects at low mass and incomplete containment of the decay products within the jet cone at high masses. Finally, the observable N_2^1, based on 2- and 3-point energy correlation functions of the jet constituents, is used to select jets consistent with a two-pronged topology [28]. The variable is explicitly decorrelated from m_{SD} and p_T using the design decorrelated tagger method [29], defining:

$$N_2^{1,DDT}(\rho, p_T) \equiv N_2^1(\rho, p_T) - X_{(5\%)}(\rho, p_T), \tag{4.1}$$

where $X_{(5\%)}(\rho, p_T)$ is the value of N_2^1 corresponding to 5% efficiency for the QCD background in a particular bin (ρ, p_T). Events with $N_2^{1,DDT} < 0$ constitute the signal, or "pass" region, while events with $N_2^{1,DDT} > 0$ form the "fail" region. To improve the statistical precision of the computation of the quantiles, the method employs a gaussian kernel estimate: QCD events at generator level are "smeared" using a parametrization of the detector resolution in N_2^1 and ρ as a function of p_T (accounting for correlations between the variables), multiplying the quantities at generator level by a random number taken from a Gaussian distribution so that the smeared distributions match those obtained from the full detector simulation.

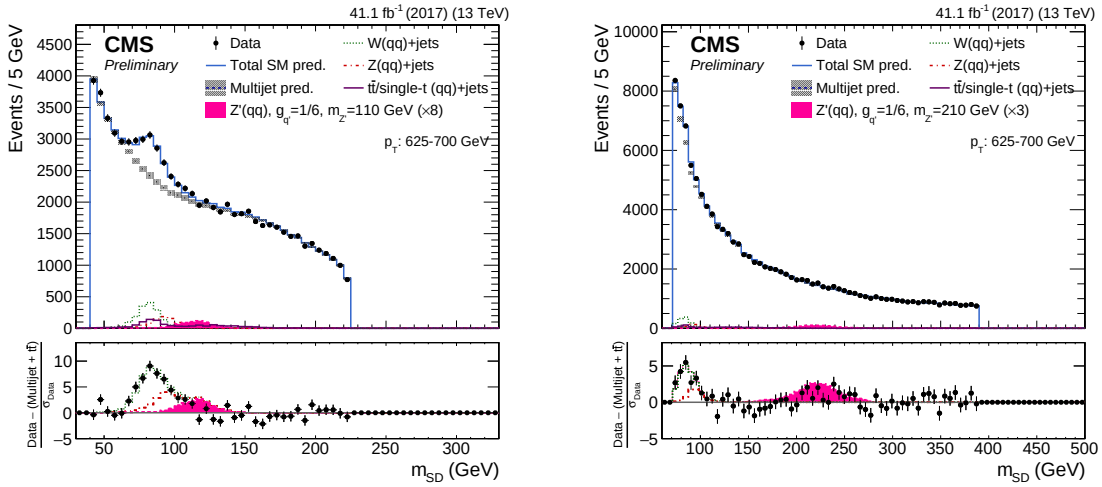

Figure 5: The m_{SD} distribution in data for AK8 (left) and CA15 (right) jets for the 625 GeV – 700 GeV p_T category of the fit. Data are shown as black points. The multijet background prediction, including uncertainties, is shown by the shaded bands. Contributions from the W and Z bosons and the top quark background processes are shown. A hypothetical Z′ boson signal with a mass of 110 GeV and coupling $g'_q = \frac{1}{6}$ is also indicated. The signal is scaled by a factor of 8 for clarity. In the bottom panel, the ratio of the data to its statistical uncertainty, after subtracting the nonresonant backgrounds, is shown. The signal is stacked on top of the peak formed by merged W and Z profiles.

The predictions of resonant backgrounds due to SM W and Z production are taken from simulation, as is that due to $t\bar{t}$. The dominant QCD background is estimated from data events with $N_2^{1,DDT} > 0$. By construction, in simulation, the QCD mass and p_T distributions are the same in

events with $N_2^{1,\mathrm{DDT}} > 0$ and $N_2^{1,\mathrm{DDT}} < 0$. To account for differences between data and simulation, the shape is multiplied by a polynomial transfer factor. Specifically, the QCD prediction is given by:

$$n_{\mathrm{pass}}^{\mathrm{QCD}}(\rho, p_{\mathrm{T}}) = R_{\mathrm{p/f}}(\rho, p_{\mathrm{T}}) n_{\mathrm{fail}}^{\mathrm{QCD}}(\rho, p_{\mathrm{T}}), \tag{4.2}$$

where $R_{\mathrm{p/f}}(\rho, p_{\mathrm{T}})$ is a polynomial in ρ and p_{T}. The order of the polynomial is minimized using a Fisher F-test procedure, to limit the bias on the fitted signal strengths. A simultaneous fit is performed to all the p_{T} categories and the pass and fail regions, with the QCD shape in the fail region and the parameters of the polynomial left freely floating. The observed m_{SD} spectra for AK8 and CA15 jets in the transverse momentum range 625 GeV – 700 GeV are shown in figure 5, along with the predicted backgrounds and example signals. No significant excesses are observed, and limits on the coupling g'_q are shown in figure 6. The jet type, AK8 or CA15, is chosen based on the expected sensitivity: CA15 jets are used above 225 GeV, while AK8 jets are used below.

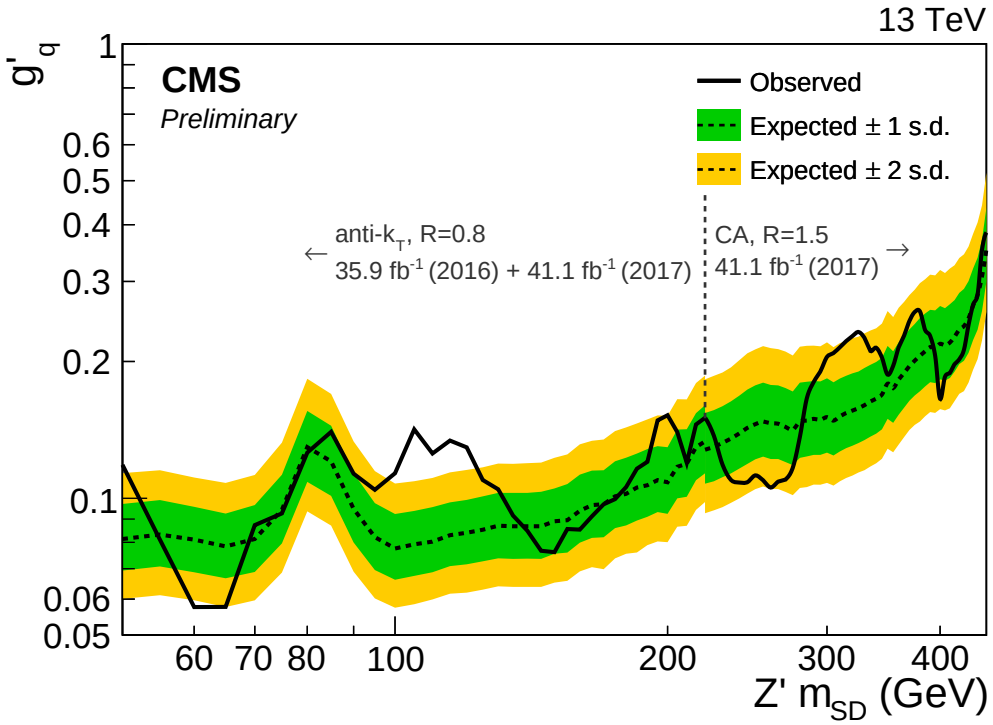

Figure 6: The upper limits at 95% CL on the coupling g'_q as a function of resonance mass for a leptophobic Z′ resonance that only couples to quarks. For masses between 50 and 220 GeV the limits correspond to a Z′ resonance reconstructed using the AK8 jet algorithm, using 77.0 fb^{-1} of statistically combined data from 2016 and 2017. The excess in the observed limit over the expected limit near 120 GeV is a remnant of the analysis of the data collected in 2016. For masses from 220 GeV to 450 GeV, the limits correspond to a Z′ resonance reconstructed using the CA15 jet algorithm, using 41.1 fb^{-1} of data collected in 2017.

5. Boosted dijet search with ISR photons

Using ISR jets to evade trigger limitations, the previously described search is able to probe dijet resonances with masses down to 50 GeV. The threshold can be lowered even further using ISR photons, which have a much lower p_T requirement in the trigger. We now describe a search for Z' bosons produced with significant photon ISR, probing the mass range 10 GeV – 125 GeV [14]. The search uses 35.9 fb^{-1} of data collected in 2016.

Events for the analysis are recorded using triggers that require a photon with $p_T > 175$ GeV and $|\eta| < 3.0$. The analysis requires the photon to have $p_T > 200$ GeV and $|\eta| < 2.4$, in order to have a constant trigger efficiency. Events with $|\eta| < 2.1$ form the signal region, while events with $2.1 < |\eta| < 2.4$ are used as a control region for the N_2^1 decorrelation, described below. The analysis uses AK8 jets reconstructed from PF candidates, using the PUPPI algorithm to reduce the impact of pileup. The jet with the highest transverse momentum is chosen as the signal jet candidate, and is required to have $p_T > 200$ GeV. The background contribution from $t\bar{t}$ is reduced by vetoing events with missing transverse momentum greater than 75 GeV, or containing an AK4 jet with $p_T > 30$ GeV and satisfying the loose working point of the CSVv2 b tagging algorithm [30]. Finally, the photon and the signal jet are required to be well-separated, satisfying $\sqrt{\Delta\eta^2 + \Delta\phi^2} > 2.2$.

As with the previous analysis, the soft-drop algorithm with $\beta = 0$ and $z_{cut} = 0.1$ is applied to the signal jet to reduce the mass of jets arising from quarks and gluons. The decorrelated N_2^1 variable is used to select jets with two-pronged substructure:

$$N_2^{1,\mathrm{DDT}}(\rho, p_T) = N_2^1(\rho, p_T) - X_{(10\%)}(\rho, p_T). \tag{5.1}$$

Here, $X_{(10\%)}(\rho, p_T)$ is the 10^{th} percentile of N_2^1 in the corresponding (ρ, p_T) bin, computed using the control sample of events with photon pseudorapidity in the range $2.1 < |\eta| < 2.4$. A K-nearest neighbors smoothing algorithm is applied to the control sample to mitigate unphysical results in bins with limited statistics.

The backgrounds due to SM $W + \gamma$, $Z + \gamma$, and $t\bar{t}$ are taken from simulation, as are the Z' signal shapes. The QCD background is estimated using equation 4.2, where $R_{p/f}$ now accounts for differences in the pass/fail ratio between the signal and control regions defined by the photon η.

A simultaneous fit is performed to the pass and fail m_{SD} distributions, with the QCD shape in the fail region and the coefficients of $R_{p/f}$ left freely floating. The observed m_{SD} distribution in the signal region is shown in figure 7, along with the predicted backgrounds and example signal distributions. No signficiant excess is observed, and limits are set on the coupling constant g'_q of the Z' model. The limits on g'_q are shown in figure 8.

6. Conclusion

We have presented three searches for dijet resonances covering a broad range of resonance masses. For masses above 2400 GeV, we have introduced a new background estimation method which uses events in a sideband of jet pairs with large pseudorapidity separation. The method has reduced systematic uncertainty, and therefore better sensitivity, compared to the method based on empirical fits to the invariant mass spectrum commonly used to date. For masses below 450 GeV, where the event rate due to QCD multijet production exceeds the trigger bandwidth, searches for

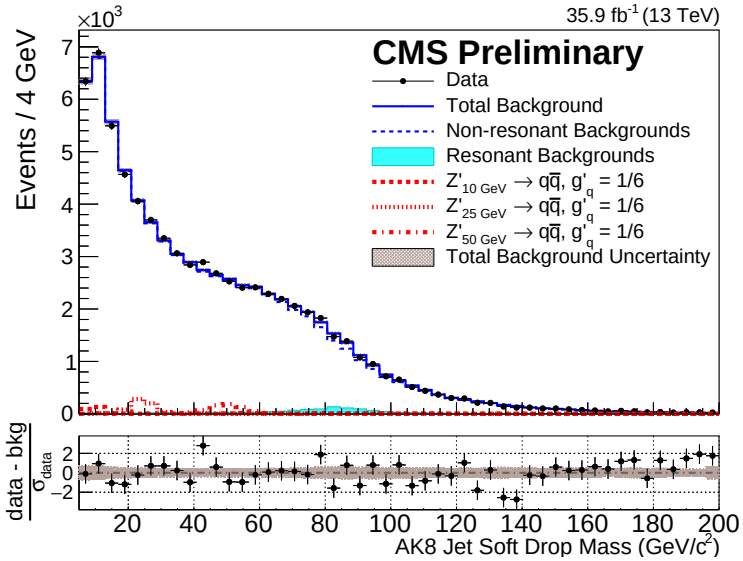

Figure 7: The soft drop jet mass distribution of the signal region after the main background estimation fit is performed. The nonresonant background is indicated by a dashed line, while the total background composed of the sum of this nonresonant background and the resonant backgrounds is shown by the solid line. Representative signals are plotted for comparison. The bottom panel shows the difference between the data and the final background estimate, divided by the statistical uncertainty of the data in each bin. The shaded region represents the total uncertainty in the background estimate in each bin.

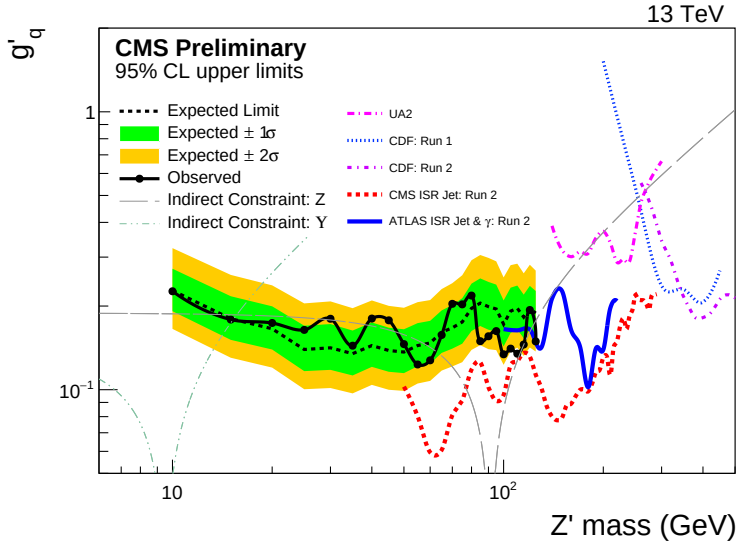

Figure 8: Upper limits at 95% CL on the coupling strength g'_q of $Z' \to q\bar{q}$. The observed limit is shown as a solid black line, while the expected limit is dashed. The green (dark) and yellow (light) bands represent 1 and 2 standard deviation intervals. Limits from other searches and the indirect constraint from measurements of the Υ and Z boson decay widths are also shown.

resonances produced with significant ISR have extended the mass range covered by LHC dijet searches down to 10 GeV. The two searches presented, targeting resonances produced with either an ISR photon or an ISR jet, have demonstrated the best sensitivity in the mass range 10 GeV – 50 GeV and 10 GeV – 50 GeV and 50 GeV – 250 GeV, respectively.

References

[1] E. Eichten et al. "Supercollider physics". In: *Rev. Mod. Phys.* 56 (4 Oct. 1984), pp. 579–707. DOI: 10.1103/RevModPhys.56.579. URL: https://link.aps.org/doi/10.1103/RevModPhys.56.579.

[2] Bogdan A. Dobrescu and Felix Yu. "Coupling-mass mapping of dijet peak searches". In: *Phys. Rev. D* 88 (3 Aug. 2013), p. 035021. DOI: 10.1103/PhysRevD.88.035021. URL: https://link.aps.org/doi/10.1103/PhysRevD.88.035021.

[3] U. Baur, I. Hinchliffe, and D. Zeppenfeld. "Excited Quark Production at Hadron Colliders". In: *Int. J. Mod. Phys.* A2 (1987), p. 1285. DOI: 10.1142/S0217751X87000661.

[4] U. Baur, M. Spira, and P. M. Zerwas. "Excited-quark and -lepton production at hadron colliders". In: *Phys. Rev. D* 42 (3 Aug. 1990), pp. 815–824. DOI: 10.1103/PhysRevD.42.815. URL: https://link.aps.org/doi/10.1103/PhysRevD.42.815.

[5] Lisa Randall and Raman Sundrum. "An Alternative to Compactification". In: *Phys. Rev. Lett.* 83 (23 Dec. 1999), pp. 4690–4693. DOI: 10.1103/PhysRevLett.83.4690. URL: https://link.aps.org/doi/10.1103/PhysRevLett.83.4690.

[6] Robert M. Harris and Konstantinos Kousouris. "Searches for Dijet Resonances at Hadron Colliders". In: *Int. J. Mod. Phys.* A26 (2011), pp. 5005–5055. DOI: 10.1142/S0217751X11054905. arXiv: 1110.5302 [hep-ex].

[7] CMS Collaboration. "Search for narrow and broad dijet resonances in proton-proton collisions at $\sqrt{s} = 13$ TeV and constraints on dark matter mediators and other new particles". In: *JHEP* 08 (2018), p. 130. DOI: 10.1007/JHEP08(2018)130. arXiv: 1806.00843 [hep-ex].

[8] Morad Aaboud et al. "Search for new phenomena in dijet events using 37 fb^{-1} of pp collision data collected at $\sqrt{s}$ =13 TeV with the ATLAS detector". In: *Phys. Rev.* D96.5 (2017), p. 052004. DOI: 10.1103/PhysRevD.96.052004. arXiv: 1703.09127 [hep-ex].

[9] Vardan Khachatryan et al. "Search for narrow resonances in dijet final states at $\sqrt{(s)} = 8$ TeV with the novel CMS technique of data scouting". In: *Phys. Rev. Lett.* 117.3 (2016), p. 031802. DOI: 10.1103/PhysRevLett.117.031802. arXiv: 1604.08907 [hep-ex].

[10] M. Aaboud et al. "Search for low-mass dijet resonances using trigger-level jets with the ATLAS detector in pp collisions at $\sqrt{s} = 13$ TeV". In: *Phys. Rev. Lett.* 121.8 (2018), p. 081801. DOI: 10.1103/PhysRevLett.121.081801. arXiv: 1804.03496 [hep-ex].

[11] CMS Collaboration. "Search for narrow resonances in the b-tagged dijet mass spectrum in proton-proton collisions at $\sqrt{s} = 8$ TeV". In: *Phys. Rev. Lett.* 120.20 (2018), p. 201801. DOI: 10.1103/PhysRevLett.120.201801. arXiv: 1802.06149 [hep-ex].

[12] Bogdan A. Dobrescu and Claudia Frugiuele. "Hidden GeV-scale interactions of quarks". In: *Phys. Rev. Lett.* 113 (2014), p. 061801. DOI: 10.1103/PhysRevLett.113.061801. arXiv: 1404.3947 [hep-ph].

[13] CMS Collaboration. "Search for low mass vector resonances decaying into quark-antiquark pairs in proton-proton collisions at $\sqrt{s} = 13$ TeV". In: (2019). arXiv: 1909.04114 [hep-ex].

[14] CMS Collaboration. "Search for low-mass quark-antiquark resonances produced in association with a photon at $\sqrt{s} = 13$ TeV". In: (2019). arXiv: 1905.10331 [hep-ex].

[15] *Searches for dijet resonances in pp collisions at* $\sqrt{s} = 13$ TeV *using the 2016 and 2017 datasets*. Tech. rep. CMS-PAS-EXO-17-026. Geneva: CERN, 2018. URL: http://cds.cern.ch/record/2637847.

[16] CMS Collaboration. "The CMS experiment at the CERN LHC". In: *Journal of Instrumentation* 3.08 (Aug. 2008), S08004–S08004. DOI: 10.1088/1748-0221/3/08/s08004. URL: https://doi.org/10.1088/1748-0221/3/08/s08004.

[17] CMS Collaboration. "Particle-flow reconstruction and global event description with the CMS detector". In: *JINST* 12.10 (2017), P10003. DOI: 10.1088/1748-0221/12/10/P10003. arXiv: 1706.04965 [physics.ins-det].

[18] Matteo Cacciari, Gavin P Salam, and Gregory Soyez. "The anti-ktjet clustering algorithm". In: *Journal of High Energy Physics* 2008.04 (Apr. 2008), pp. 063–063. DOI: 10.1088/1126-6708/2008/04/063. URL: https://doi.org/10.1088/1126-6708/2008/04/063.

[19] Yu.L Dokshitzer et al. "Better jet clustering algorithms". In: *Journal of High Energy Physics* 1997.08 (Aug. 1997), pp. 001–001. DOI: 10.1088/1126-6708/1997/08/001. URL: https://doi.org/10.1088/1126-6708/1997/08/001.

[20] Matteo Cacciari, Gavin P. Salam, and Gregory Soyez. "FastJet user manual". In: *The European Physical Journal C* 72.3 (Mar. 16, 2012), p. 1896. ISSN: 1434-6052. DOI: 10.1140/epjc/s10052-012-1896-2. URL: https://doi.org/10.1140/epjc/s10052-012-1896-2.

[21] "Jet energy scale and resolution performance with 13 TeV data collected by CMS in 2016". In: (June 2018). URL: http://cds.cern.ch/record/2622157.

[22] CMS Collaboration. "Pileup mitigation at CMS in 13 TeV data". In: (2019).

[23] CMS Collaboration. "Search for low mass vector resonances decaying into quark-antiquark pairs in proton-proton collisions at $\sqrt{s} = 13$ TeV". In: *JHEP* 01 (2018), p. 097. DOI: 10.1007/JHEP01(2018)097. arXiv: 1710.00159 [hep-ex].

[24] ATLAS Collaboration. "Search for light resonances decaying to boosted quark pairs and produced in association with a photon or a jet in protonproton collisions at s=13TeV with the ATLAS detector". In: *Physics Letters B* 788 (2019), pp. 316–335. ISSN: 0370-2693. DOI: https://doi.org/10.1016/j.physletb.2018.09.062. URL: http://www.sciencedirect.com/science/article/pii/S037026931830830X.

[25] ATLAS Collaboration. "Search for low-mass resonances decaying into two jets and produced in association with a photon using pp collisions at s=13 TeV with the ATLAS detector". In: *Physics Letters B* 795 (2019), pp. 56–75. ISSN: 0370-2693. DOI: https://doi.org/10.1016/j.physletb.2019.03.067. URL: http://www.sciencedirect.com/science/article/pii/S0370269319303612.

[26] David Krohn, Jesse Thaler, and Lian-Tao Wang. "Jet Trimming". In: *JHEP* 02 (2010), p. 084. DOI: 10.1007/JHEP02(2010)084. arXiv: 0912.1342 [hep-ph].

[27] Andrew J. Larkoski et al. "Soft Drop". In: *JHEP* 05 (2014), p. 146. DOI: 10.1007/JHEP05(2014)146. arXiv: 1402.2657 [hep-ph].

[28] Ian Moult, Lina Necib, and Jesse Thaler. "New Angles on Energy Correlation Functions". In: *JHEP* 12 (2016), p. 153. DOI: 10.1007/JHEP12(2016)153. arXiv: 1609.07483 [hep-ph].

[29] James Dolen et al. "Thinking outside the ROCs: Designing Decorrelated Taggers (DDT) for jet substructure". In: *JHEP* 05 (2016), p. 156. DOI: 10.1007/JHEP05(2016)156. arXiv: 1603.00027 [hep-ph].

[30] CMS Collaboration. "Identification of heavy-flavour jets with the CMS detector in pp collisions at 13 TeV". In: *JINST* 13.05 (2018), P05011. DOI: 10.1088/1748-0221/13/05/P05011. arXiv: 1712.07158 [physics.ins-det].